Infrared Physics & Technology 59 (2013) 137–141

Contents lists available at SciVerse ScienceDirect

Infrared Physics & Technology

journal homepage: www.elsevier.com/locate/infrared

Concept of infrared photodetector based on graphene–graphene nanoribbon structure

Victor Ryzhii [a,c,e,*], Taiichi Otsuji [a,c], Nadezhda Ryabova [b,c], Maxim Ryzhii [b,c], Vladimir Mitin [d], Valeriy Karasik [e]

[a] Research Institute of Electrical Communication, Tohoku University, Sendai 980-8577, Japan
[b] Computational Nanoelectronics Laboratory, University of Aizu, Aizu-Wakamatsu 965-8580, Japan
[c] Japan Science and Technology Agency, CREST, Tokyo 107-0075, Japan
[d] Dept. of Electrical Engineering, University at Buffalo, Buffalo, NY 14260-1920, USA
[e] Center for Photonics and Infrared Engineering, Bauman Moscow State Technical University, Moscow 105005, Russia

HIGHLIGHTS

- We study the mechanisms of photoconductivity in graphene layer-graphene nanoribbon-graphene layer (GL-GNR-GL) structures.
- We develop the device model for GL-GNR-GL photodiode.
- The GL-GNR-GL photodiodes can effectively detect infrared and terahertz radiation at room temperature.

ARTICLE INFO

Article history:
Available online 29 December 2012

Keywords:
Infrared detector
Graphene
Graphene nanoribbon
Photocurrent
Dark current

ABSTRACT

We study the mechanisms of photoconductivity in graphene layer–graphene nanoribbon–graphene layer (GL–GNR–GL) structures with the *i*-type gapless GL layers as sensitive elements and *I*-type GNRs as barrier elements. The effects of both an increase in the electron and hole densities under infrared illumination and the electron and hole heating and cooling in GLs are considered. The device model for a GL–GNR–GL photodiode is developed. Using this model, the dark current, photocurrent, and responsivity are calculated as functions of the structure parameters, temperature, and the photon energy. The transition from heating of the electron–hole plasma in GLs to its cooling by changing the incident photon energy can result in the change of the photoconductivity sign from positive to negative. It is demonstrated that GL–GNR–GL photodiodes can be used in effective infrared and terahertz detectors operating at room temperature. The change in the photoconductivity sign can be used for the discrimination of the incident radiation with the wavelength 2–3 μm and 8–12 μm.

1. Introduction

Due to the gapless energy spectrum, graphene [1] absorbs electromagnetic radiation from the terahertz to ultraviolet spectral range (see, for instance, Refs. [2–4]). The fairly high quantum efficiency of the interband transitions in graphene [2] and particularly in multiple-graphene layer structures [5] promotes the creation of novel effective infrared (IR) and terahertz (THz) photodetectors. Several concepts of IR/THz photodetectors, utilizing graphene single-and multiple layer structures as well as graphene nanoribbon structures (photoconductors, photodiodes, and phototransistors), have been proposed, evaluated, and studied experimentally [6–15]. In the photodiodes and phototransistors based on graphene nanoribbon structures considered previously [8,16], these structures play the role of the absorbing region. However, to achieve appropriate responsivity in such devices, a large number of relatively long GNRs (about the wavelength of incident radiation) or special optical antenna are required. In this paper, we consider graphene photodetectors which comprise two undoped (*i*-type) gapless graphene layers (GLs) (absorbing regions supplied by the side contacts) and connected with each other by a graphene nanoribbon (GNR) or an array of GNRs with a finite band gap (undoped wide-gap barrier region of the *I*-type). The device structure of such a graphene layer–graphene nanoribbon–graphene layer (GL–GNR–GL) photodiode under consideration and its energy diagram are shown in Fig. 1. In this device, the incident radiation is absorbed by GLs. This results in an increase in the electron and hole densities in these regions. The latter leads to an increase of the thermionic

* Corresponding author at: Research Institute of Electrical Communication, Tohoku University, Sendai 980-8577, Japan.
E-mail address: v-ryzhii@riec.tohoku.ac.jp (V. Ryzhii).

1350-4495/$ - see front matter © 2012 Elsevier B.V. All rights reserved.
http://dx.doi.org/10.1016/j.infrared.2012.12.028

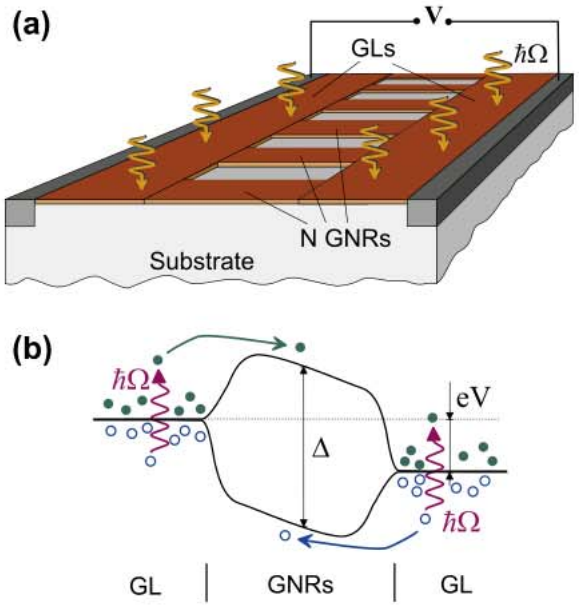

Fig. 1. Schematic views of (a) GL–GNR–GL photodiode and (b) its energy diagram under bias voltage V (wavy arrows correspond to interband transitions due to absorption of photons in GLs, smooth arrows indicate propagation of electrons and holes above the pertinent barriers in GNRs).

electron and hole currents across the energy barrier formed in GNRs, i.e., to the appearance of the photocurrent. The presence of the GNR(s) and the pertinent energy barrier provides an opportunity to control (reduce) the dark current. In illuminated GLs, a marked portion of the absorbed optical energy goes to the electron and hole energies. This can normally result in a heating of the electron–hole system and, hence, in an extra increase in the current over the barrier. The variation of the current associated with the deviation of the electron and hole temperature T from its equilibrium value T_0 can be pronounced. However, the situation can be even more complex. At elevated ($T_0 \gtrsim 100$ K) temperatures, in contrast to what is going on at low temperatures [6], the interband transitions associated with optical phonons can be the dominant mechanism of the recombination [17]. The energy relaxation of electrons and holes in GLs can also be mainly due to interaction with optical phonons [18]. As a result, the optical photons emitted by the photogenerated electrons and holes can accumulate in GLs. This implies the heating of the optical phonon system. The deviation of the optical phonon system from equilibrium can also affect the interband generation–recombination processes. The latter can lead to both the heating the the electron–hole system and its cooling depending on the energy of incident photons $\hbar\Omega$ adding complexity to the photodetector spectral characteristics. Thus, the accounting for the optical phonon heating appears to be indispensable [19,20].

2. GL–GNR–GL photodiode model and the pertinent equations

We consider the undoped device structure shown in Fig. 1 with a symmetrical electron–hole system i.e., the GLs and GNRs are undoped. The width of GNRs is chosen to provide necessary energy gap Δ; It is assumed that the intraband absorption in GLs and the interband absorption in GNRs are insignificant (this issue is discussed in the end of the paper). The intercarrier scattering time is sufficiently short to provide fast maxwellisation (fermisation) of the photogenerated electrons and holes. We also believe that the intraband and interband (generation and recombination) relaxation is associated with optical phonons (of one type), that corresponds to a high temperature (room or somewhat lower temperatures) operation.

In such a situation, the electron and hole distribution functions in GLs are equal and given by $f = \{\exp[(\varepsilon - \varepsilon_F)/T] + 1\}^{-1}$. Here $\varepsilon = v_W p$ is the energy of electrons and holes with the momentum p, $v_W = 10^8$ cm/s is the characteristic velocity of the GL energy spectrum, ε_F is the quasi-Fermi energy, and T is the effective temperature (in the energy units). In the case under consideration, the optical phonon system can also be far from equilibrium, so that the distribution function of optical phonons $\mathcal{N}_0$ can markedly deviate from its equilibrium value $\mathcal{N}_0^{eq} = [\exp(\hbar\omega_0/T_0) - 1]^{-1}$, where $\hbar\omega_0 \simeq 200$ meV is the energy of optical phonon in GLs.

The quasi-Fermi energy of the electron–hole plasma ε_F, its effective temperature T, and the number of optical phonons $\mathcal{N}_0$ obey the equations presented as [19,20]

$$R_0^{inter} = G_\Omega, \tag{1}$$

$$\hbar\omega_0\left(R_0^{inter} + R_0^{intra}\right) = G_\Omega \hbar\Omega, \tag{2}$$

$$\hbar\omega_0\, R^{decay} = \hbar\Omega\, G_\Omega. \tag{3}$$

These equations govern the balance of the electron–hole pairs, the balance of the energy of the electron–hole system, respectively, as well as the optical phonon balance. Here, R_0^{inter}, R_0^{intra}, and R^{decay} are the rates of the pertinent processes. Eq. (3) explicitly takes into account that all the energy received by the system from radiation goes eventually to the thermostat. Neglecting the effect of Pauli blocking at the interband optical transitions, the rate of optical generation of electron–hole pairs is given by [21]

$$G_\Omega = \pi\alpha\, \tanh\left(\frac{\hbar\Omega}{4T}\right) I. \tag{4}$$

Here, I is the photon flux of radiation and $\alpha \simeq 1/137$ is the fine structure constant (so that the absorption coefficient is equal to $\pi\alpha \simeq 0.023$).

As previously [19,20], for the terms R_0^{inter} and R_0^{intra}, we use the following simplified expressions:

$$R_0^{inter} = \frac{\Sigma_0}{\tau_0^{inter}}\left[(\mathcal{N}_0 + 1)\exp\left(\frac{2\varepsilon_F - \hbar\omega_0}{T}\right) - \mathcal{N}_0\right], \tag{5}$$

$$R_0^{intra} = \frac{\Sigma_0}{\tau_0^{intra}}\left[(\mathcal{N}_0 + 1)\exp\left(-\frac{\hbar\omega_0}{T}\right) - \mathcal{N}_0\right]. \tag{6}$$

Here, $\Sigma_0 = \pi(T_0/\hbar v_W)^2/6$ is the equilibrium electron and hole density, $\tau_0^{inter} \propto \tau_0^{intra} \propto \tau_0$ are the times of the interband and intraband phonon-assisted processes, and τ_0 is the characteristic time of spontaneous emission of optical phonon. Some difference in τ_0^{inter} and τ_0^{intra} is mainly associated with the features of the density of states. In equilibrium, i.e., at $\mathcal{N}_0 = \mathcal{N}_0^{eq}$, $\varepsilon_F = 0$, and $T = T_0$, from Eqs. (6) and (7) one obtains $R_0^{inter} = R_0^{intra} = 0$.

The rate of optical phonons decay due to the anharmonic contributions to the interatomic potential, resulting in the phonon–phonon scattering and in the decay of optical phonons into acoustic phonons and is assumed to be in the following form:

$$R_0^{decay} = \frac{\Sigma_0(\mathcal{N}_0 - \mathcal{N}_0^{eq})}{\tau_0^{decay}}, \tag{7}$$

where τ_0^{decay} is the pertinent characteristic time. Considering high heat conductivity of GLs [22], the lattice temperature, i.e. the temperature of acoustic phonons, is assumed to be equal to the temperature of the contact T_0.

3. Variations of effective temperature and quasi-Fermi energy under illumination

Solving Eqs. (1), (3), and (7), we obtain

$$\mathcal{N}_0 - \mathcal{N}_0^{eq} = \mathcal{N}_0^{eq}\eta_0^{decay}\left(\frac{\Omega}{\omega_0}\right)\tanh\left(\frac{\hbar\Omega}{4T}\right)\frac{I}{I_0}. \quad (8)$$

Here we have introduced the characteristic photon flux

$$I_0 = \mathcal{N}_0^{eq}\frac{\Sigma_0}{\pi\alpha\tau_0^{inter}} \simeq \exp\left(-\frac{\hbar\omega_0}{T_0}\right)\frac{\omega_0}{\Omega}\frac{\Sigma_0}{\pi\alpha\tau_0^{inter}},$$

and the parameter $\eta_0^{decay} = \tau_0^{decay}/\tau_0^{inter}$.

For the relatively low intensities of incoming radiation (so that T is close to T_0 and ε_F is close to zero), from Eqs. (1)–(8), we arrive at

$$\frac{T - T_0}{T_0} \simeq \frac{T_0}{\hbar\omega_0}\left|\eta_0^{decay}\left(\frac{\Omega}{\omega_0}\right) + \eta_0^{eq}\left(\frac{\Omega}{\omega_0} - 1\right)\right|\tanh\left(\frac{\hbar\Omega}{4T_0}\right)\frac{I}{I_0}, \quad (9)$$

$$\frac{\varepsilon_F}{T_0} \simeq \frac{1}{2}\left|1 - \eta_0^{eq}\left(\frac{\Omega}{\omega_0} - 1\right)\right|\tanh\left(\frac{\hbar\Omega}{4T_0}\right)\frac{I}{I_0}. \quad (10)$$

Here we have introduced the parameter $\eta_0 = \tau_0^{intra}/\tau_0^{inter}$. At $\varepsilon_F < T$, one obtains $\eta_0 = \eta_0^{eq} \simeq (\hbar\omega_0/\pi\, T_0)^2/(1 + 2.19T_0/\hbar\omega_0)$, so that at $T_0 = 300$ K, $\eta_0^{eq} \simeq 5$ [19].

As follows from Eq. (9), the effective temperature increases (the electron and hole heating) with increasing I in the radiation frequency range $\Omega > \omega_0\left(1 - \eta_0^{decay}/\eta_0\right)$ and decreases when $\Omega < \omega_0\left(1 - \eta_0^{decay}/\eta_0\right)$. Setting $\eta_0 = 5$ and $\eta_0^{decay} = 1$–3 [17], we find that at these parameters the heating of the electron–hole system changes to its cooling at a certain photon energy $\hbar\Omega_0$, where the latter is in the range $\hbar\Omega = \hbar\Omega_0 = 80$–$160$ meV. In the case of instantenieous decay of nonequilibrium optical phonons $\left(\eta_0^{decay} = 0\right)$ due to, say, their interaction with phonons in the substrate, the cooling of the electron–hole system occurs at $\hbar\Omega_0 = 200$ meV. This is because when $\eta_0^{decay} = 0$, i.e., the optical phonon system does not deviate from equilibrium, every act of the electron and hole photogeneration supplies the electron–hole plasma with the energy $\hbar\Omega$, while every act of recombination (due to the emission of optical phonons) decreases the energy of electron hole plasma by the value of $\hbar\omega_0$. When η_0^{decay} is finite, some heating of the optical phonon system occurs. The interaction of electrons and holes with a hot (or warm) optical phonon system contributes some heating of the electron–hole plasma. The change in the quasi-Fermi energy sign takes place when Ω becomes larger than $\omega_0(1 + \eta_0^{-1})$. Assuming $\eta_0 = 5$, we find that the freezing out of the electron–hole plasma (decrease in its density under the effect of illumination) is possible if $\Omega > 6\omega_0/5$, i.e., when $\hbar\Omega > 360$ meV. It is instructive, that a decrease in the electron–hole plasma density occurs when $T > T_0$. This is because an increase in T leads to an increase in the rate of recombination involving optical phonons.

4. Dark current and photocurrent

Consider the devices with sufficiently narrow GNRs in which the majority of electrons and holes are concentrated in the lowest subband of the conduction band and the topmost subband of the valence band. Taking into account the one-dimensional electron and hole transport in GNRS, the sum of the electron and hole currents through N parallel GNRs is equal to

$$J = \frac{8eN}{2\pi\hbar} \times \int_{\Delta_B}^{\infty} d\varepsilon_{GNR}\left\{\left|\exp\left(\frac{\varepsilon_{GNR} - \varepsilon_F}{T}\right) + 1\right|^{-1} - \exp\left|\left(\frac{\varepsilon_{GNR} - \varepsilon_F - eV}{T}\right) + 1\right|^{-1}\right\}. \quad (11)$$

Here e is the absolute value of the electron charge, ε_{GNR}= is the dispersion low or electrons and holes in GNR, and $\Delta_B = \Delta_{B0} - eaV \simeq \Delta/2 - eaV$, where $\Delta_{B0} \simeq \Delta/2$ is the barrier height when $V = 0$, $\Delta \propto 2\pi\hbar v_W/d$ is the energy gap in GNRs, d is the GNR width, and $a < 1/2$ is a positive coefficient determined by the effect of barrier lowering under the applied bias voltage $V > 0$ (the barrier form factor). For a parabolic barrier $a \simeq 1/2$, while for a smooth barrier (long GNR), this coefficient can be markedly smaller.

After the integration, Eq. (11) can be presented as

$$J = \frac{4eNT}{\pi\hbar}\left\{\ln\left|\exp\left(\frac{\varepsilon_F - \Delta_B}{T}\right) + 1\right| - \ln\left|\exp\left(\frac{\varepsilon_F - \Delta_B - eV}{T}\right) + 1\right|\right\} \simeq \frac{4eNT}{\pi\hbar}\exp\left(\frac{\varepsilon_F - \Delta_B}{T}\right)\left|1 - \exp\left(-\frac{eV}{T}\right)\right|. \quad (12)$$

As follows from Eq. (12), the current in the absence of illumination J_0 (dark current) is given by

$$J_0 \simeq \frac{4eT_0N}{\pi\hbar}\exp\left(-\frac{\Delta}{2T_0}\right)\exp\left(\frac{eaV}{T_0}\right)\left|1 - \exp\left(-\frac{eV}{T_0}\right)\right|. \quad (13)$$

Assuming $\Delta = 50$ meV, $V = 50$ mV, $a = 1/2$, and $N = 1$, for $T_0 = 200$–300 K from Eq. (13) we obtain $J_0 \simeq (3.47$–$4.56) \times 10^{-6}$ A. An increase in the GNR energy gap Δ leads to a significant drop of the dark current. At small values of the barrier form-factor a, the voltage dependence of the dark current becomes rather weak at $eV > T_0$.

Since $(T - T_0)/T_0$ and ε_F/T_0 are small, the variation of the current through one GNR $J - J_0$ (photocurrent), can be presented in the following form:

$$J - J_0 \simeq \frac{4eN}{\pi\hbar}\exp\left(-\frac{\Delta}{2T_0}\right)\exp\left(\frac{eaV}{T_0}\right)\left|1 - \exp\left(-\frac{eV}{T}\right)\right|\left|\left(\frac{\Delta - eaV}{T_0} + 1\right)(T - T_0) + \varepsilon_F\right|. \quad (14)$$

Substituting the expressions for $T - T_0$ and ε_F given by Eqs. (9)–(14), we obtain

$$J - J_0 \simeq \frac{4eNT_0}{\pi\hbar}\exp\left(-\frac{\Delta}{2T_0}\right)\exp\left(\frac{eaV}{T_0}\right)\left|1 - \exp\left(-\frac{eV}{T}\right)\right| \times \left|\left(\frac{\Delta/2 + T_0 - eaV}{\hbar\omega_0}\right)\frac{\Omega}{\omega_0}\eta_0^{decay} + \eta_0\left(\frac{\Delta/2 + T_0 - eaV}{\hbar\omega_0} - \frac{1}{2}\right)\left(\frac{\Omega}{\omega_0} - 1\right) + \frac{1}{2}\right| \times \tanh\left(\frac{\hbar\Omega}{4T_0}\right)\frac{I}{I_0}. \quad (15)$$

5. Responsivity

Using Eq. (15) for the responsivity $R_J = (J - J_0)/S\hbar\Omega\, I$ of a photodiode with N GNRs and the GL areas S, one can find

$$R_J \simeq NR_J^0\exp\left(\frac{eaV}{T_0}\right)\left|1 - \exp\left(-\frac{eV}{T_0}\right)\right| \times \left|\left(\frac{\Delta/2 + T_0 - eaV}{\hbar\omega_0}\right)\frac{\Omega}{\omega_0}\eta_0^{decay} + \eta_0\left(\frac{\Delta/2 + T_0 - eaV}{\hbar\omega_0} - \frac{1}{2}\right)\left(\frac{\Omega}{\omega_0} - 1\right) + \frac{1}{2}\right| \times \tanh\left(\frac{\hbar\Omega}{4T_0}\right). \quad (16)$$

Here

$$R_J^0 = \left(\frac{4e}{\pi\hbar\, SI_0}\right)\left(\frac{T_0}{\hbar\Omega}\right)\exp\left(-\frac{\Delta}{2T_0}\right) = \left(\frac{4\alpha\tau_0^{inter}e}{\hbar\Sigma_0 S}\right)\left(\frac{T_0}{\hbar\omega_0}\right)\exp\left(\frac{\hbar\omega_0}{T_0}\right)\exp\left(-\frac{\Delta}{2T_0}\right). \quad (17)$$

The quantity $(\Sigma_0/\tau_0^{inter})\exp(-\hbar\omega_0/T_0) = G_0^{eq}$ is the rate of the interband generation of electron- hole pairs due to the absorption of optical phonons in graphene in equilibrium. Expressing R_J^0 via G_0^{eq}, Eq. (17) can be presented in the following form:

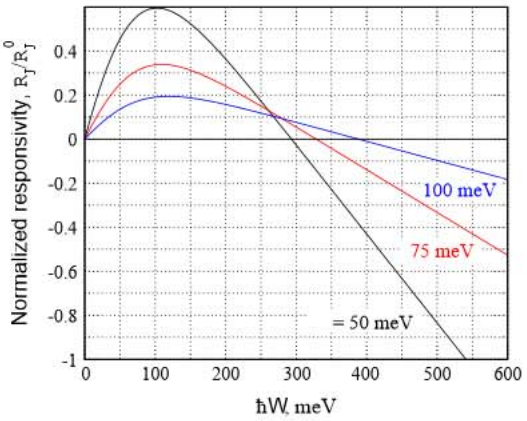

Fig. 2. Spectral dependences of normalized responsivity of a GL–GNR–GL photodiode with single GNR ($N = 1$) at different values of the GNR energy gap Δ.

$$R_J^0 = \left(\frac{4\alpha\, e}{\hbar\, G_0^{eq} S}\right)\left(\frac{T_0}{\hbar\omega_0}\right). \tag{18}$$

At $T_0 = 300$ K it can be estimated as [17] $G_0^{eq} = 10^{21}$ cm^{-2} s^{-1}. Assuming $S \simeq \lambda^2/2 = 0.5 \times 10^{-6}$ cm^2 (λ is the radiation wavelength) and $\Delta = 50$ meV, we obtain $R_J^0 \simeq 1.16 \times 10^{-2}$ A/W. Setting $a = 1/2$, $\eta_0^{decay} = 1$–3 [19], $\hbar\Omega = 100$ meV, and $V = 50$ mV, we obtain $R_J \simeq (2.5\text{–}3.0) \times 10^{-2}$ A/W. One can see that at the parameters under consideration, the photocurrent is positive (the current increases with increasing intensity of radiation).

The characteristic responsivity R_J^0 as well as R_J dramatically increase with decreasing temperatures if $\Delta < 2\hbar\omega_0 \simeq 400$ meV. This, first of all, is associated with a drastic (exponential) decrease in the rate of the optical phonon mechanism of recombination and generation (factor G_0^{eq} in Eq. (18)). As the dark current, the responsivity is a weak function of the voltage if $eV > T_0$.

One can see from Eq. (17) that the responsivity is a function of Ω changing its sign at a certain frequency Ω_1. For $\eta_0^{decay} = 0$, 1, and 3 one obtains $\hbar\Omega_1 = 253$, 267, and 293 meV, respectively. The cases when $\Omega < \Omega_1$ correspond to $R_J > 0$, i.e., to the positive photoconductivity, while when $\Omega > \Omega_1$, $R_J < 0$ (negative photoconductivity). The latter is attributed to the effect of substantial increase in the rate of recombination with the emission of optical phonons when the energy received by the electro-hole system from radiation (proportional to $\hbar\Omega$) becomes sufficiently large.

Fig. 2 shows the spectral dependences of the normalized responsivity R_J/R_J^0 of a GL–GNR–GL photodiode with $N = 1$ calculated for different values of the energy gap Δ in GNRs. It is assumed that $T_0 = 300$ K, $a = 0.1$, $\eta_0^{decay} = 1$, $\eta_0 = 5$, and $V = 100$ mV.

6. Discussion of the results

As follows from Eqs. (15) and (16) and seen from Fig. 2, the spectral dependences of photoconductivity and responsivity change their signs when the energy of incident photons decreases. In particular, for the photon energies $\hbar\Omega = 100$–150 meV ($\lambda \simeq 8$–12 μm) the responsivity is positive $R_J > 0$, while for $\hbar\Omega = 400$–600 meV ($\lambda \simeq 2$–3 μm) it becomes negative. This can be used for the discrimination of the incident radiation in different ranges of infrared spectrum. The detector responsivity can be markedly increase by using the GL–GNR–GL structures with multiple GNRs ($N \gg 1$).

Choosing parameter Δ, i.e., the GNR width, one can control the value of the dark current, and, hence, the detector dark-current limited detectivity $D^* \propto R_J/\sqrt{J_0} \propto \exp(-\Delta/4T_0)\sqrt{N}$. Thus, increase in number of GNRs N leads to an increase in both the responsivity and the detectivity.

The intraband (Drude) absorption of incident radiation can also change the effective temperature of the electron–hole plasma in GLs. This can lead to a change in the plasma density (due to the temperature dependence of the recombination rate) and in the current. The relative role of the latter (bolometric) mechanism can be characterized the parameter $\beta = \mathrm{Re}\,\sigma_\Omega^{intra}/\mathrm{Re}\,\sigma_\Omega^{inter}$, where $\mathrm{Re}\,\sigma_\Omega^{inter}$ and $\mathrm{Re}\,\sigma_\Omega^{inter}$ are the real parts of the GL dynamic conductivities associated with the intraband and interband transitions, respectively. Considering that the Fermi energy $\varepsilon_F = 0$, this parameter is estimated as (see, for instance [19])

$$\beta = \frac{4\pi}{3}\left(\frac{\hbar v_0}{T_0}\right)\frac{T_0^2}{\hbar^2\left(\Omega^2 + v_0^2\right)\tanh(\hbar\Omega/4T_0)}, \tag{19}$$

where ν_0 is the collision frequency of electrons and holes. The condition $\beta \ll 1$ is satisfied except the low end of the THz range. For example, assuming that $T_0 = 300$ K and $\nu_0 = 10^{12}$ s^{-1} and setting $\hbar\Omega \gtrsim 25$ meV, we obtain β [0.1. At smaller radiation frequencies (a few THz) and less perfect GLs (with larger ν_0), β can be markedly larger exceeding unity. This implies that in the latter cases the intraband absorption can provide essential contribution. The operation of THz detectors based on gated heterostructures made of A_3B_5 compounds associated with the heating of two-dimensional electron gas due to the intraband absorption of THz was discussed in Refs. [23–25].

The incident radiation is absorbed in GNRs if $\hbar\Omega > \Delta$. This can also be utilized in GNR-based photodetectors [16]. However, the efficiency of such detectors drops when the GNR length l becomes shorter that the radiation wavelength λ. As a result, a marked contribution of GNR section to the incident radiation absorption can occur if the number of GNRs in this section is large and they are sufficiently long or an optical antenna is provided.

Above, we focused on GL–GNR–GL photodiodes with undoped GLs. The structures with doped GLs of n- and p-types (i.e., with ε_F 0) can also be used for IR and THz photodetection. The main difference in GL–GNR–GL photodiodes with undoped and doped GLs is in substantially different spectra of radiation absorption and, hence, the detector spectral characteristics. This is due to the Pauli blocking of the interband absorption of low energy photons with $\hbar\Omega < 2\varepsilon_F$, where the Fermi energy in doped GLs is determined by the dopant concentration (or by the applied voltage in the structures with special gates).

7. Conclusions

We considered the effect of photoconductivity in a GL–GNR–GL photodiode using its developed device model. The dark current, photocurrent, and responsivity were calculated as functions of the structure parameters and temperature, as well as their spectral characteristics. As shown, the GL–GNR–GL photodiodes can be used in effective infrared and terahertz detectors operating at room temperature. The predicted effect of different sign of the photoconductivity in different spectral ranges can be used for the discrimination of the incident radiation with the wavelength 2–3 μm and 8–12 μm.

Acknowledgment

The work was supported by the Japan Science and Technology Agency, CREST, The Japan Society for Promotion of Science, Japan, and by the TERANO-NSF Grant, USA.

References

[1] A.H. Castro Neto, F. Guinea, N.M.R. Peres, K.S. Novoselov, A.K. Geim, The electronic properties of graphene, Rev. Mod. Phys. 81 (2009).

[2] F. Bonnaccorso, Z. Sun, T. Hasan, A.C. Ferrari, Graphene photonics and optoelectronics, Nat. Photonic. 4 (2010) 611.
[3] R.R. Nair, P. Blake, A.N. Grigorenko, K.S. Novoselov, T.J. Booth, T. Stauber, N.M.R. Peres, A.K. Geim, Fine structure constant defines visual transparency of graphene, Science 320 (2008) 1308.
[4] J.M. Dawlaty, S. Shivaraman, J. Strait, P. George, M. Chandrashekhar, F. Rana, M.G. Spencer, D. Veksler, Y. Chen, Measurement of the optical spectra of epitaxial fraphene from terahertz to visible, Appl. Phys. Lett. 93 (2008) 131905.
[5] M. Orlita, M. Potemski, Dirac electronic states in graphene systems: optical spectroscopy studies, Semicond. Sci. Technol. 25 (2010) 063001.
[6] F.T. Vasko, V. Ryzhii, Photoconductivity of an intrinsic graphene, Phys. Rev. B 77 (2008) 195433.
[7] A. Satou, F.T. Vasko, V. Ryzhii, Nonequilibrium carriers in intrinsic graphene under interband photoexcitation, Phys. Rev. B 78 (2008) 115431.
[8] V. Ryzhii, V. Mitin, M. Ryzhii, N. Ryabova, T. Otsuji, Device model for graphene nanoribbon phototransistor, Appl. Phys. Express 1 (2008) 063002.
[9] V. Ryzhii, M. Ryzhii, Graphene bilayer field-effect phototransistor for terahertz and infrared detection, Phys. Rev. B 79 (2009) 245311.
[10] J. Park, Y.H. Ahn, C. Ruiz-Vargas, Imaging of photocurrent generation and collection in single-layer graphene, Nano Lett. 9 (2009) 1742.
[11] F. Xia, T. Murller, Y.-M. Lin, A. Valdes-Garsia, F. Avouris, Ultrafast graphene photodetector, Nat. Nanotechnol. 4 (2009) 839–843.
[12] V. Ryzhii, M. Ryzhii, V. Mitin, T. Otsuji, Terahertz and infrared photodetection using p–i–n multiple-graphene structures, J. Appl. Phys. 106 (2009) 084512.
[13] T. Mueller, F. Xia, P. Avouris, Graphene photodetectors for high-speed optical communications, Nat. Photon. 4 (2010) 297.
[14] V. Ryzhii, M. Ryzhii, N. Ryabova, V. Mitin, T. Otsuji, Terahertz and infrared detectors based on graphene structures, J. Infrared Phys. Technol. 54 (2011) 302–305.
[15] M. Ryzhii, T. Otsuji, V. Mitin, V. Ryzhii, Characteristics of p–i–n terahertz and infrared photodiodes based on multiple graphene layer structures, Jpn. J. Appl. Phys. (STAP) 50 (2011) 070117.
[16] V. Ryzhii, N. Ryabova, M. Ryzhii, N.V. Baryshnikov, V.E. Karasik, V. Mitin, T. Otsuji, Terahertz and infrared photodetectors based on multiple graphene layer and nanoribbon structures, Optoelectron. Rev. 20 (2012) 15.
[17] F. Rana, P.A. George, J.H. Strait, S. Shivaraman, M. Chanrashekhar, M.G. Spencer, Carrier recombunation and generation rates for intravalley and intervalley phonon scattering in graphene, Phys. Rev. B 79 (2009) 115447.
[18] R.S. Shishir, D.K. Ferry, S.M. Goodnick, Room temperature velocity saturation in intrinsic graphene, J. Phys.: Conf. Ser. 193 (2009) 012118.
[19] V. Ryzhii, M. Ryzhii, V. Mitin, A. Satou, T. Otsuji, Effect of heating and cooling of photogenerated electronhole plasma in optically pumped graphene on population inversion, Jpn. J. Appl. Phys. 50 (2011) 094001.
[20] V. Ryzhii, M. Ryzhii, V. Mitin, T. Otsuji, Toward the creation of terahertz graphene injection laser, J. Appl. Phys. 110 (2011) 094503.
[21] L.A. Falkovsky, A.A. Varlamov, Space-time dispersion of graphene conductivity, Eur. Phys. J. B 56 (2007) 281.
[22] A.A. Balandin, S. Ghosh, D.L. Nika, E.P. Pokatilov, Thermal conduction in suspended graphene layers, Fullerenes, Nanotubes Carbon Nanostructures 18 (2010) 474.
[23] X.G. Peralta, S.J. Allen, M.C. Wanke, N.E. Harff, J.A. Simmons, M.P. Lilly, J.L. Reno, P.J. Burke, J.P. Eisenstein, Terahertz photoconductivity and plasmon modes in double-quantum-well field-effect transistors, Appl. Phys. Lett. 81 (2002) 1627.
[24] E.A. Shaner, M. Lee, M.C. Wanke, A.D. Grine, J.L. Reno, S.J. Allen, Single-quantum-well grating-gated terahertz plasmon detectors, Appl. Phys. Lett. 87 (2005) 193507.
[25] V. Ryzhii, A. Satou, T. Otsuji, M.S. Shur, Plasma mechanisms of resonant terahertz detection in a two-dimensional electron channel with split gates, J. Appl. Phys. 103 (2008) 014504.